Interface morphology of a Cr(001)/Fe(001) superlattice determined by scanning tunneling microscopy and x-ray diffraction: A comparison

C. M. Schmidt, D. E. Bürgler,[a] D. M. Schaller, F. Meisinger, and H.-J. Güntherodt
Institut für Physik, Universität Basel, Klingelbergstrasse 82, CH-4056 Basel, Switzerland

K. Temst
Laboratorium voor Vaste-Stoffysika en Magnetisme, Katholieke Universiteit Leuven, Celestijnenlaan 200 D, B-3001 Leuven, Belgium

(Received 19 April 2000; accepted for publication 11 October 2000)

A Cr(001)/Fe(001) superlattice with ten bilayers grown by molecular beam epitaxy on a Ag(001) substrate is studied by *in situ* scanning tunneling microscopy (STM) and *ex situ* x-ray diffraction (XRD). Layer-resolved roughness parameters determined from STM images taken in various stages of the superlattice fabrication are compared with average values reported in the literature or obtained from the fits of our XRD data. Good agreement is found for the rms roughnesses describing *vertical* roughness and for the *lateral* correlation lengths characterizing correlated as well as uncorrelated interface roughness if peculiarities of STM and XRD are taken into account. We discuss in detail (i) the possible differences between the STM topography of a free surface and the morphology of a subsequently formed interface, (ii) contributions due to chemical intermixing at the interfaces, (iii) the comparison of XRD parameters averaged over all interfaces *versus* layer-resolved STM parameters, and (iv) the question of the coherent field of view for the determination of rms values.
© *2001 American Institute of Physics.* [DOI: 10.1063/1.1330770]

I. INTRODUCTION

Magnetic multilayers reveal fascinating physical properties as giant magnetoresistance (GMR)[1,2] and oscillatory magnetic interlayer exchange coupling.[3–5] Both phenomena are known to be highly structure sensitive. In particular, thickness fluctuations of the nonferromagnetic interlayers resulting from uncorrelated interface roughness crucially affect the exchange coupling properties[6,7] or give rise to biquadratic coupling,[8] and GMR depends on the quality of the interfaces due to its origin from spin-dependent interface scattering.[9] Interface roughness in general must be characterized by a whole set of parameters such as rms roughness (always associated to some sampling length measured within the plane of the interface), in-plane correlation lengths, terrace sizes and shapes, profiles of atomic intermixing, atomic displacements, and many more depending on the specific interface.

Two main courses for the characterization of the interfaces in metallic layered structures have been followed: (i) x-ray diffraction (XRD) is a widely spread technique that allows the characterization of buried interfaces, but usually requires a minimum number of the order of ten interfaces to yield sufficient signal intensities. The resulting interface parameters (correlation lengths, interface widths, and chemical intermixing profiles) represent an averaged interface and also depend on the model assumptions plugged into the fitting procedure. (ii) Imaging by scanning tunneling microscopy (STM)—or any other scanning probe technique such as atomic force microscopy (ATM)—provides very detailed direct-space information about a free surface that only after measuring—upon deposition of a subsequent film of a different material—will transform into a buried interface. Hence, the information gained by STM describes one single interface and strongly relies on the assumption that the morphology of a buried interface is sufficiently well described by the corresponding initial free surface. The high degree of structural detail information obtained by STM comes at the cost of low statistics compared to XRD due to its nature as a near-field technique. Obviously, the combined use of both complementary techniques STM and XRD promises strong advantages to get more reliable interface characterizations, e.g., by using a roughness model derived from STM images as the starting point of the fitting procedure for the XRD data analysis.

In this article we present a combined *in situ* STM and *ex situ* XRD study of a $[\mathrm{Cr}(001)/\mathrm{Fe}(001)]_{10}$ multilayer. We discuss interface roughness parameters deduced from direct-space images of the various surfaces occurring during sample fabrication and complement our findings with subsurface sensitive diffraction measurements performed with the very same sample after completion of its superlattice structure.

The Cr(001)/Fe(001) superlattice is a suitable and physically relevant model system for such a comparative study: Oscillatory magnetic interlayer coupling and GMR have both been discovered in Cr/Fe layered structures, and since then Cr/Fe has served as a model systems in the field of thin film magnetism. Much effort has already been put into the characterization of the interfaces by different techniques, among them STM[6,7] and XRD,[11] and interesting properties such as

[a]Author to whom correspondence should be addressed; Present address: Institut für Festkörperforschung, Forschungszentrum Jülich GmbH, Germany; electronic mail: D.Buergler@fz-juelich.de

 © 2001 American Institute of Physics

Downloaded 02 Oct 2001 to 148.6.178.100. Redistribution subject to AIP license or copyright, see http://ojps.aip.org/japo/japcr.jsp

interface alloying affecting the phase and strength of interlayer coupling,[12,13] subtle correlations between interface morphology and interlayer coupling,[6,7] and an increase of the GMR effect with increasing interface roughness[14,15] have been reported.

II. EXPERIMENT

Sample preparation and all measurements, with the exception of XRD, are performed in an UHV system with a base pressure of 5×10^{-11} mbar that is equipped with a molecular beam epitaxy deposition system, UHV–STM, low-energy electron diffraction (LEED), Auger and x-ray photoemmission electron spectroscopy (AES, XPS), and an *in situ* magnetooptical Kerr effect (MOKE) setup that we operate in the longitudinal configuration.

A 150-nm-thick Ag(001) buffer layer grown on Fe-precovered GaAs(001) wafers at $T_S=380$ K and postannealed at $T_A=570$ K serves as substrate system for the magnetic multilayer. We have previously presented a detailed investigation of the morphological properties of the Ag(001) buffer layer:[16] STM images reveal terraces with a mean width of approximately 35 nm that are separated by monatomic steps. Most of these steps originate from screw dislocations which are found to be the representative kind of defect in this substrate system. Meanwhile we have been able to extend the average Ag terrace width by about a factor of three by using GaAs(001) wafers which are passivated by an amorphous As cap instead of oxidized GaAs(001) substrates.[17]

The multilayer itself consists of ten repetitions of Cr(001)/Fe(001) grown at room temperature at a deposition rate of 0.01 nm/s. We intermit the preparation process at various stages to take STM, MOKE, and/or LEED data. The *nominal* layer thickness (in contrast to the one measured by *ex situ* XRD) is monitored by a quartz microbalance; for the Fe films the nominal thickness reads 5 nm, whereas for the Cr layers it amounts to 2.5 nm. Fe(001)/Cr(001)/Fe(001) trilayers with wedge-shaped Cr spacers grown at elevated temperatures are expected to exhibit interlayer exchange coupling oscillations with a periodicity in Cr thickness very close to 2 ML≈0.29 nm.[5] By verifying these 2 ML oscillations using MOKE measurements on trilayer samples prepared accordingly[7] we estimate the absolute error of the nominal thickness measurement to be on the order of ±10%, whereas the relative reproducibility proves to be better than ±5%. The cleanness of the layers is confirmed by XPS and AES. All morphological, chemical, and magnetic characterizations are performed at room temperature.

For the *ex situ* XRD analysis the sample is coated with a 5-nm-thick Ag protection layer. The XRD experiments are carried out by $\theta-2\theta$ scans on a Rigaku diffractometer with a 12 kW rotating anode and using Cu $K\alpha$ radiation ($\lambda=0.154$ nm). The diffractometer is equipped with a post-sample crystal monochromator and a Ni filter. The multilayer samples are mounted on a thin-film attachment. The step size of the measured data was 0.01°, and a scintillation counter was used as a detector.

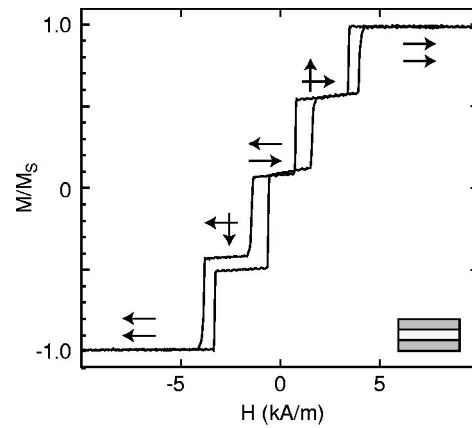

FIG. 1. Longitudinal MOKE magnetization curve of the $[Cr(001)/Fe(001)]_{10}$ sample in the intermediate trilayer stage of preparation (see Ref. 10). The external magnetic field is applied parallel to a ⟨100⟩ magnetic easy axis of the Fe(001) layers. Arrows indicate the relative orientation of the magnetizations of the Fe layers.

III. RESULTS

Figure 1 shows a MOKE loop in units of the saturation magnetization M_S measured *in situ* after stopping the preparation process at the trilayer level. The contour of the magnetization curve is typical for Fe(001)/Cr(001)/Fe(001) trilayers grown at room temperature on the Ag(001)/Fe/GaAs(001) substrate system with a Cr thickness in the range between 2 and 3 nm.[7] It reveals a characteristic plateau at $M/M_S\approx0$ reflecting antiferromagnetic interlayer exchange coupling at small external fields and two other plateaus at $M/M_S\approx\pm0.5$ resulting from 90° alignment of the magnetization vectors at intermediate fields as indicated by the pairs of arrows.

The comparison of the LEED patterns of the Ag(001) substrate [Fig. 2(a)] and of the completed $[Cr(001)/Fe(001)]_{10}$ superlattice [Fig. 2(b)] confirms the single crystalline quality of the entire structure. The epitaxial relationship reads as follows: the bcc–Cr(001)⟨100⟩ axes and the bcc–Fe(001)⟨100⟩ axes are parallel to each other and also parallel to the fcc–Ag(001)⟨110⟩ axes.

STM overview and detail images are recorded from the sample in various stages of preparation: An STM overview image (i.e., an image with a scan area of 400×400 nm^2) of the bottom Fe film is shown in Fig. 3(a). The shape and

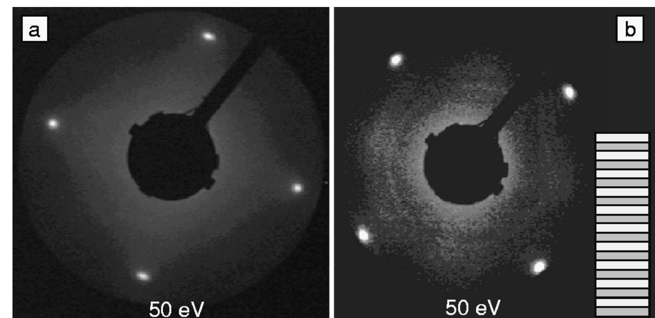

FIG. 2. (1×1) LEED patterns taken at 50 eV: (a) Ag(001) substrate and (b) top Cr(001) film of the complete $[Cr(001)/Fe(001)]_{10}$ multilayer (see Ref. 10). The patterns are displayed with an arbitrary relative orientation.

Downloaded 02 Oct 2001 to 148.6.178.100. Redistribution subject to AIP license or copyright, see http://ojps.aip.org/japo/japcr.jsp

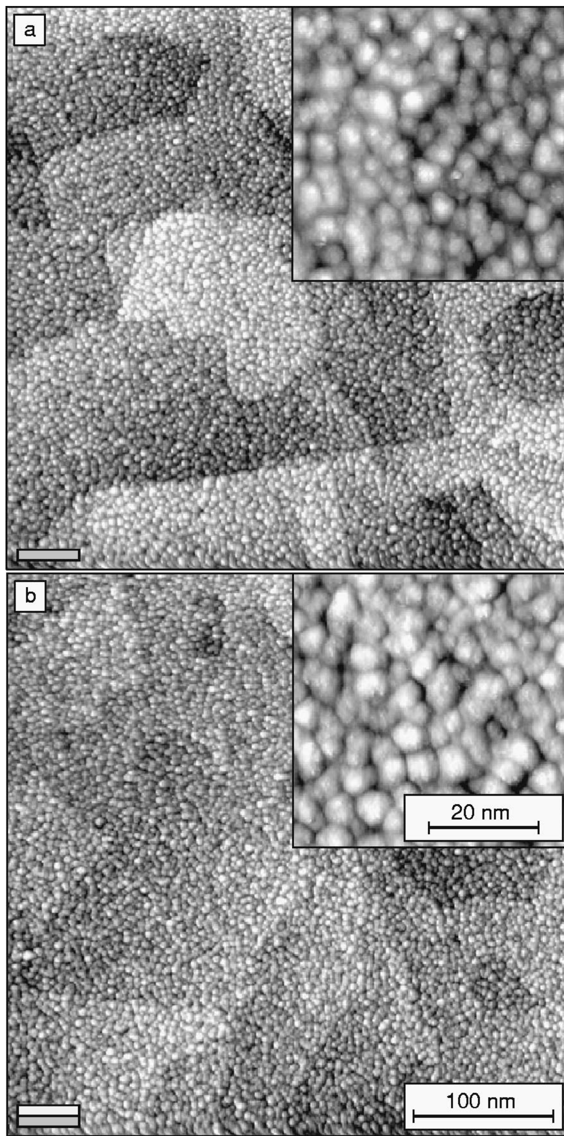

FIG. 3. STM overview images (image size: 400×400 nm^2) of various Fe and Cr surfaces occurring in the preparation process of the $[Cr(001)/Fe(001)]_{10}$ multilayer grown on the Ag(001)/Fe/GaAs(001) substrate system. Insets: detail images (50×50 nm^2). (a) Fe (z range: 1.0 nm), (b) Cr/Fe (z range: 1.0 nm). The derivative along the fast scan direction has been added to the plane-subtracted raw data for contrast enhancement (see Ref. 10).

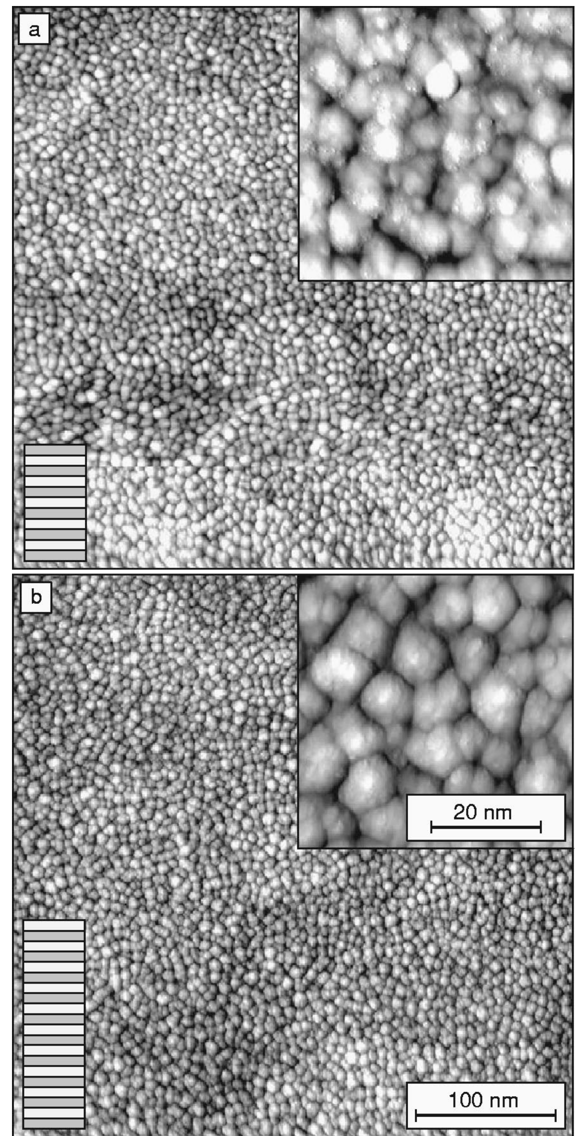

FIG. 4. STM overview images (image size: 400×400 nm^2) of various Fe and Cr surfaces occurring in the preparation process of the $[Cr(001)/Fe(001)]_{10}$ multilayer grown on the Ag(001)/Fe/GaAs(001) substrate system. Insets: detail images (50×50 nm^2). (a) $Fe/[Cr/Fe]_5$ (z range: 1.5 nm), (b) $[Cr/Fe]_{10}$ (z range: 2.0 nm). The derivative along the fast scan direction has been added to the plane-subtracted raw data for contrast enhancement (see Ref. 10).

arrangement of the large-scale contrast are very similar to the step structure of the bare Ag(001) substrate, and hence, it is induced by the substrate. However, the terraces in between two substrate-induced steps are neither structureless nor flat. The surface is covered with hillocks as revealed by the detail image (i.e., an image with a scan area of 50×50 nm^2) in the inset. We statistically quantify the *vertical* roughness of overview and detail images by calculating the rms value $\sigma = \sqrt{\langle z^2 \rangle}$, and the *lateral* roughness of detail images by calculating the lateral correlation length R. The latter quantity is determined by the position of the nearest-neighbor maximum in the pair correlation function

$$\mathrm{PCF}(r) = \frac{1}{2\pi}\int_0^{2\pi} H(r,\vartheta)\, d\vartheta, \tag{1}$$

where

$$H(r,\vartheta) = H(\boldsymbol{r}) = \frac{1}{A}\int_A z(\boldsymbol{\rho})z(\boldsymbol{\rho}+\mathbf{r})\, d^2\rho \tag{2}$$

is the two-dimensional height-height correlation function derived from the surface profiles $z(\boldsymbol{r})$ of STM images. Thus, R corresponds to the mean separation between typical features, i.e., the average distance of two adjacent hillocks. The offset of $z(\boldsymbol{r})$ is such that $\langle z \rangle = 0$. Therefore, with the normalization chosen in Eqs. (1) and (2) $\mathrm{PCF}(0) = \sigma^2$ holds.

As discussed in Ref. 18 Fe grows on Ag(001) at room temperature as a continuous, single-crystalline film with a rough surface. For the data presented in the inset of Fig. 3(a) $R_{\mathrm{Fe}} = 6.2$ nm and $\sigma_{\mathrm{Fe}}^{\mathrm{detail}} = 0.13$ nm.

Downloaded 02 Oct 2001 to 148.6.178.100. Redistribution subject to AIP license or copyright, see http://ojps.aip.org/japo/japcr.jsp

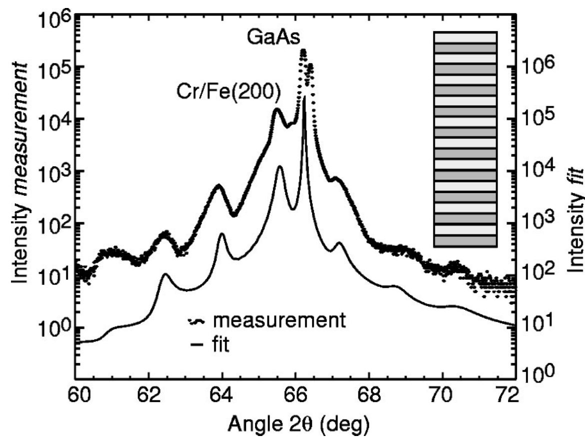

FIG. 5. High-angle x-ray diffraction spectrum of the $[Cr_{2.5\,nm}/Fe_{5\,nm}]_{10}$ multilayer grown on the Ag(001)/Fe/GaAs(001) substrate system. The left vertical axis belongs to the upper graph (measurement), the right one to the vertically shifted best fit. The fit nicely reproduces position, number, and relative intensity of the bilayer satellites (see Ref. 10).

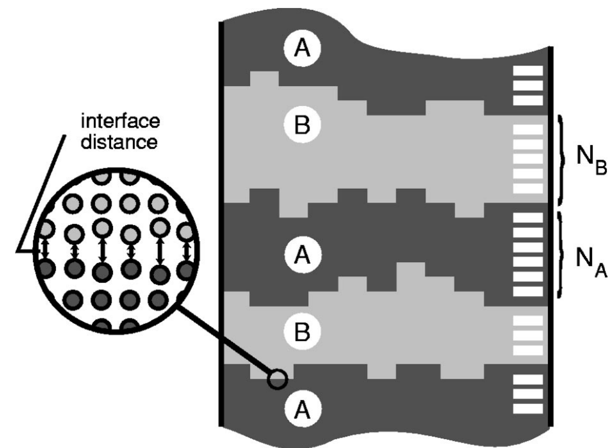

FIG. 6. Schematic drawing of the structure model used for the simulation and fitting of the XRD patterns.

Figures 3(b) and 4(a) depict images of the first Cr layer and the sixth Fe layer, respectively, and Fig. 4(b) shows the tenth Cr layer, i.e., the surface after completion of the multilayer. Generally, from the appearance of the STM data, it is impossible to distinguish between Fe and Cr surfaces: all morphologies are dominated by a rough, irregular structure due to growth hillock as demonstrated by the respective detail images in the insets.

The upper curve in Fig. 5 shows the measured $\theta-2\theta$ high-angle XRD spectrum of the sample on a logarithmic scale (vertical axis on the left-hand side). The highest apex in the pattern is produced by the GaAs(001) substrate. Its splitting into two peaks comes from the x-ray beam that is not perfectly monochromatic but includes contributions from both the Cu $K\alpha_1$ and the Cu $K\alpha_2$ lines, which differ in wavelength by 0.25%. Note that these two peaks are almost two orders of magnitude stronger than the peaks produced by the multilayer. To the left of the GaAs signal the bcc–Cr/Fe(002) fundamental peak can be observed. The periodic modulation of the superlattice is demonstrated by the equidistant first to third-order superlattice peaks that are visible on both sides of the main peak.

The lower graph displays the best fit to the data, which has been analyzed using the Suprex modeling and fitting program described in Ref. 19. Imperfections in the multilayer are included by introducing a number of parameters, as schematically shown in Fig. 6. For crystalline layers, roughness is included by assuming the presence of random variations in the number of monolayers in the crystalline layer (indicated by N_A and N_B for materials A and B, respectively). These fluctuations are, therefore, named discrete, i.e., quantized in steps equal to the lattice spacing and are presumed to have a Gaussian distribution. Furthermore, it is assumed that there can be a fluctuation of the interface distance, i.e., the vertical distance between two dissimilar atoms at the interface between two layers. For high-angle XRD data, Suprex allows a fitting of the patterns by relying on a one-dimensional kinematical structure model, implying that lateral correlations are not included.

In Fig. 5, for clarity the fitted curve is vertically shifted below the measured curve by one order of magnitude (vertical axis on the right-hand side). An additional spectrum obtained from a pure Ag(001)/Fe/GaAs(001) sample allows to separately fit and subtract the substrate contribution. Taking into account only the Cu $K\alpha_1$ line and using the STM data in setting the range of reasonable roughness values for the x-ray data, we arrive at a stable solution and a fair agreement between data and fit in the sense that the position and the number of bilayer satellites are nicely reproduced as well as their relative intensities. The asymmetry in sharpness of the satellite peaks on the left and right-hand side of the Cr/Fe(002) peak is recognized, too. The fit produces identical layer separations in the growth direction for Fe and Cr, namely 0.143 nm. From the fit the average thickness of the Fe layers is determined to be 4.05 nm, whereas the average Cr thickness is 2.12 nm, i.e., the fitted average bilayer thickness measures 6.17 nm, which is 82% of the nominally deposited thickness. Calculating the model curve using the nominal thickness values derived from the quartz microbalance does not reproduce the experimental pattern in a satisfactory manner. From the best fit the average rms roughness for the Fe surfaces can be calculated as $\bar{\sigma}_{\mathrm{Fe}}^{\mathrm{XRD}}=0.431$ nm. The corresponding quantity for the Cr surfaces is $\bar{\sigma}_{\mathrm{Cr}}^{\mathrm{XRD}}=0.345$ nm.

The low-angle measurements taken from our multilayer do not exhibit distinct multilayer peaks, and it has not been possible to fit the data. The problem arises probably (i) from the fact that the atomic scattering powers of Fe and Cr are very close to each other, which diminishes the contrast between the two materials and makes it difficult for the superlattice structure to show up clearly, and (ii) from the strong substrate contribution to the total intensity that cannot be unambiguously separated from the weak multilayer signal.

IV. DISCUSSION

First, we would like to discuss the assumption that STM images of a free surface represent the morphology of a subsequently formed interface. In the case of intermixing interfaces may change during growth. It was shown by Davies *et al.*[12] by means of STM and scanning tunneling spectros-

Downloaded 02 Oct 2001 to 148.6.178.100. Redistribution subject to AIP license or copyright, see http://ojps.aip.org/japo/japcr.jsp

copy that the initial Cr growth on Fe(001) whiskers leads to the formation of a Cr–Fe alloy within the first monolayers with temperature dependent composition. At a preparation temperature $T_S = 570$ K, the first predominantly Cr layer occurs at a Cr coverage of 2–3 ML. Using angular resolved AES, Heinrich *et al.*[13] found that for $T_S = 570$ K the interface intermixing is mostly confined to the two topmost atomic Fe layers and that the degree of intermixing is nearly 50%. Therefore, intermixing is likely to occur in our sample although to a lesser degree than observed by these authors because of the lower preparation temperature, $T_S = 300$ K. However, even in the case of moderate intermixing a STM image of an Fe surface may still be regarded as an approximation of the resulting Cr/Fe interface morphology upon progressing in the multilayer fabrication, if we assume the chemically diffuse Cr/Fe interface to be centered around the STM representation of the topography of the Fe layer. Concerning our multilayer structure with alternating Cr/Fe and Fe/Cr interfaces, STM data of Cr surfaces regarded as approximations of Fe/Cr interfaces are supposed to excel the ones of the Cr/Fe interfaces by far, since chemically sharp interfaces are reported for the growth of Fe on Cr(001).[13] Hence, a detailed and quantitative comparison of STM and XRD-derived parameters characterizing the interface morphology seems legitimate.

A qualitative description of the STM images involves two different lateral length scales. The steps that cause the large-scale image contrast in Figs. 3 and 4 separate Ag buffer layer terraces which are on average *100 nm wide* and propagate through the Cr/Fe layer stack, with their distinctness vanishing during the growth of the multilayer: The sharp step structures visible in Figs. 3(a) and 3(b) transform upon progressing through the superlattice into modulations with a comparable vertical dynamic range and a wavelength of the order of several times the mean terrace width in Figs. 4(a) and 4(b). Locally, the morphologies are dominated by growth hillocks; the mean hillock separation *of the order of only a few nanometers* increases steadily by roughly a factor of 2 from the bottom Fe surface to the topmost Cr surface. A quantitative analysis of the lateral correlation lengths R confirms the latter trend: In Fig. 7, R is plotted *versus* the nominal multilayer thickness.[20] Gray rhombuses indicate Fe surfaces and white triangles symbolize Cr surfaces. Independent of the respective surface material present, R gets larger with increasing layer thickness—approximately proportional to the total multilayer thickness to the power of 0.2 (dashed curve in Fig. 7). An exemplary PCF function calculated from the topmost Cr surface [Fig. 4(b)] is provided in the inset of Fig. 7. From the inequality of the R's we can directly conclude that the interface roughnesses cannot be correlated across the layers on the lateral length scale of the growth hillocks, i.e., a few nanometers. Therefore, layer thickness fluctuations within each layer must be present. This is indirectly confirmed in our MOKE data (Fig. 1) by the clear observation of 90° coupling in the trilayer state: In the framework of Slonczewski's model[8] spacer layer thickness fluctuations are a necessary precondition for 90° coupling.

Schreyer *et al.*[11] have arrived at fair approximations for the correlated and uncorrelated lateral correlation lengths ob-

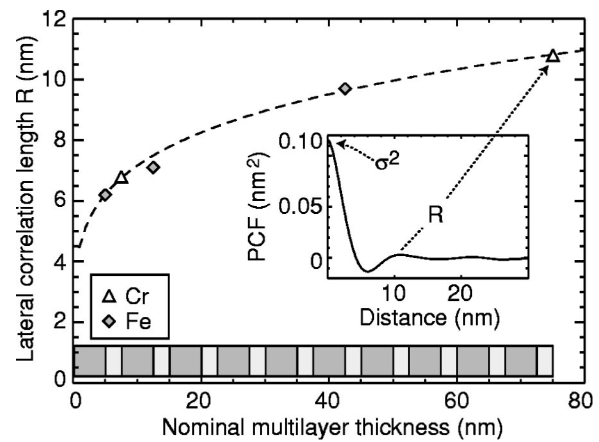

FIG. 7. Lateral correlation lengths R as a function of multilayer thickness calculated via the pair correlation function [Eqs. (1) and (2)] from STM detail images. Gray rhombuses stand for Fe data points and white triangles mark Cr data points. The dashed line is fitted to the data points and goes with the multilayer thickness to the power of 0.2. Inset: PCF calculated from the top Cr surface of the multilayer (see Ref. 10).

tained from small-angle XRD scans of a similar room temperature $[Cr_{1.7\,nm}/Fe_{5.2\,nm}]_9$ sample. In agreement with our STM findings, they encounter the presence of two lateral length scales. The smaller one (≈ 5 nm) is connected with uncorrelated roughness and corresponds to our hillock structure with R's in the range between 6 and 11 nm. The larger lateral length scale of Schreyer *et al.* (≈ 200 nm) is linked to a high degree of correlation and is attributed to the Ag substrate template, too. As mentioned by Schreyer *et al.*[11] all their absolute values may only be considered as rough order of magnitude estimates. Hence, the STM–XRD comparison of the *lateral* interface roughness parameters yields satisfactory agreement.

The STM and XRD parameters for the *vertical* roughness are displayed in Fig. 8. The averaged rms roughness values derived from our XRD measurements, $\bar{\sigma}_{Fe}^{XRD}$ and $\bar{\sigma}_{Cr}^{XRD}$, are shown as horizontal lines [smallest rhombuses (Fe) and triangles (Cr)] together with the layer-resolved data points $\sigma_{Fe,Cr} = \sqrt{PCF(0)}$ derived from the STM detail (over-

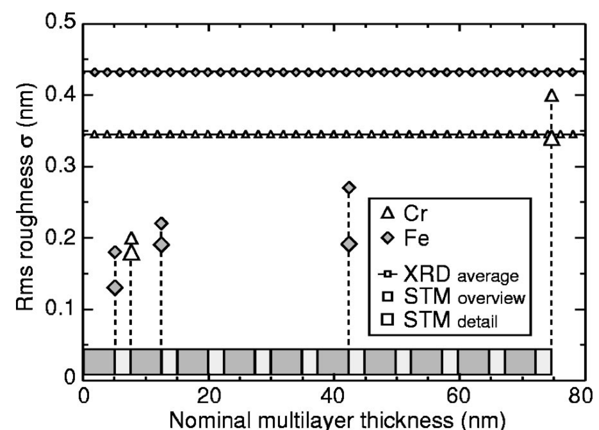

FIG. 8. rms roughnesses σ obtained from XRD measurements (small symbols), STM overview images (medium-sized symbols), and STM detail images (large symbols), plotted against the nominal multilayer thickness (see Ref. 10).

Downloaded 02 Oct 2001 to 148.6.178.100. Redistribution subject to AIP license or copyright, see http://ojps.aip.org/japo/japcr.jsp

view) images [largest (medium sized) rhombuses (Fe) and triangles (Cr)]. As it was the case for the lateral correlation length, the STM rms values increase with increasing multilayer thickness regardless of whether the respective layer surface is Fe or Cr. All values with the exception of $\sigma_{\mathrm{Cr}}^{\mathrm{overview}}$ of the complete multilayer lie below the corresponding average encountered by XRD ($\bar{\sigma}_{\mathrm{Fe,Cr}}^{\mathrm{XRD}}$). For a comparison with the XRD values one has to compute the average of all layer-resolved interface roughnesses (including those of the interfaces that have not been imaged by STM). Evidently one finds that the averaged STM-derived rms values are systematically smaller than those derived from XRD: $\overline{\sigma_{\mathrm{Fe,Cr}}^{\mathrm{overview}}} < \bar{\sigma}_{\mathrm{Fe,Cr}}^{\mathrm{XRD}}$. We explain this difference with three arguments.

First, a vertical length scale is always associated to some lateral sampling length that defines the longest wavelength of the roughness which is taken into account for the determination of roughness parameters. In STM we can tune this field of coherent view very easily just by varying the scan range. The medium-sized symbols in Fig. 8 display the rms roughnesses as calculated from the STM overview images of Figs. 3 and 4. We always find $\sigma^{\mathrm{detail}} < \sigma^{\mathrm{overview}}$. The main difference between the two sets of data is that the latter reflects to a much larger extent the Ag substrate contribution. For large multilayer thicknesses, $\sigma^{\mathrm{overview}}$ does not approach σ^{detail} implying that the influence of the Ag substrate steps does not vanish, but rather smears out upon growth, as described before. In agreement with Ref. 11 this scenario involves a high degree of correlated roughness on the length scale of the substrate terrace width. A problem with roughness parameters determined by XRD is precisely that the field of coherent view is not well-known. In textured Nb/Cu multilayers Temst *et al.*[21] have encountered a sampling length of about the grain size (45 nm) by an *ex situ* XRD and *ex situ* AFM comparison. In our single-crystalline samples the coherent field of view in the XRD experiment might still be larger than the one connected with the STM overview images (400 nm) and may thus explain the larger rms values encountered in XRD.

Second, as has also been noted before in Ref. 22, the vertical roughness values obtained from XRD refinement procedures measures deviations from the ideal multilayer structure consisting of (i) interface roughness and (ii) layer thickness variations from one layer to the next along the multilayer. The second contribution tends to increase the rms values derived from XRD as compared to the STM-derived parameters.

Third, as stressed before, surface topographies might change geometrically and/or chemically when turning into interface morphologies upon deposition of additional layers. In particular, the Cr/Fe interface—in contrast to the Fe/Cr interface—is well known to exhibit chemical intermixing. $\bar{\sigma}_{\mathrm{Fe}}^{\mathrm{XRD}} > \bar{\sigma}_{\mathrm{Cr}}^{\mathrm{XRD}}$ could reflect the chemical broadening of the Cr/Fe interface regions. The STM images do not show this trend since the actual interfaces with the chemically intermixed regions are formed after the STM measurement. Hence, chemical intermixing seems to occur. The additional roughness contribution σ_{Δ} to $\bar{\sigma}_{\mathrm{Fe}}^{\mathrm{XRD}}$ compared to $\bar{\sigma}_{\mathrm{Cr}}^{\mathrm{XRD}}$ can be calculated as

$$\sigma_{\Delta}^2 = (\bar{\sigma}_{\mathrm{Fe}}^{\mathrm{XRD}})^2 - (\bar{\sigma}_{\mathrm{Cr}}^{\mathrm{XRD}})^2. \tag{3}$$

We obtain $\sigma_{\Delta} \approx 0.258$ nm. Assuming that chemical intermixing only occurs at the Cr/Fe interface and that it causes the full difference between $\bar{\sigma}_{\mathrm{Fe}}^{\mathrm{XRD}}$ and $\bar{\sigma}_{\mathrm{Cr}}^{\mathrm{XRD}}$ we can estimate an upper bound of the effect of chemical intermixing. Depending on the detailed assumptions about the intermixing the value of σ_{Δ} corresponds to a thickness of the FeCr alloy layer at the Cr/Fe interface of approximately 3 ML. This is certainly a reasonable value for an upper limit[12,13] indicating that the surface does not undergo significant geometric changes when a subsequent layer is deposited even when modest intermixing occurs. The center of the alloy layer shows similar geometric fluctuations as the initial free surface, and chemical fluctuations due to the interface alloy simply add to the geometric fluctuations. This scenario confirms our assumption of a chemically diffuse interface which is centered at the topography of the initial free surface.

Additional XRD simulations with a single rms value and assuming an intermixed $\mathrm{Fe}_x\mathrm{Cr}_{1-x}$ layer show that the main features in the XRD pattern are more sensitive to the roughness parameters than to interdiffusion parameters. They do not provide a unique determination of thickness and composition x of the alloy layer. This is due to the fact that the XRD pattern is not changing very much and that a comparatively large number of new parameters enters the problem. The analysis is complicated because the interdiffusion causes slight changes in the intensity of the satellite peaks, which can be compensated in the fit by the very influential background from the GaAs substrate peak.

In conclusion, roughness parameters derived from STM images taken in various stages of superlattice fabrication compare well with parameters obtained from the fitting of XRD spectra of the completed structure and agree with previous XRD results of Schreyer *et al.*[11] The comparison shows that STM images of free surfaces indeed yield valuable information about the morphology of subsequently formed interfaces. Chemical intermixing occurring during interface formation leads to an alloy layer which follows the topography of the initial free surface. The width of the alloy layer leads to an additional contribution to the rms roughness measured by XRD but not by STM. The steady increase of the layer-resolved rms roughness (σ) and lateral correlation length (R) with the number of layers in the superlattice indicates that XRD-derived parameters can only be understood as averages over interfaces of with widely spread σ's and R's. The XRD rms roughness is larger than the average of the STM-derived values even for the interface type showing no chemical intermixing ($\bar{\sigma}_{\mathrm{Cr}}^{\mathrm{XRD}} > \overline{\sigma_{\mathrm{Cr}}^{\mathrm{overview}}}$). This fact points out that the coherent field of view in XRD is larger than the STM image size of $400 \times 400\ \mathrm{nm}^2$.

ACKNOWLEDGMENTS

Financial support from the Swiss National Science Foundation and the Swiss Kommission für Technologietransfer und Innovation is gratefully acknowledged. K. T. is a Postdoctoral Research Fellow of the Fund for Scientific Research—Flanders (FWO).

Downloaded 02 Oct 2001 to 148.6.178.100. Redistribution subject to AIP license or copyright, see http://ojps.aip.org/japo/japcr.jsp

[1] G. Binasch P. Grünberg, F. Saurenbach, and W. Zinn, Phys. Rev. B **39**, 4828 (1989).
[2] M. N. Baibich *et al.*, Phys. Rev. Lett. **61**, 2472 (1988).
[3] P. Grünberg, R. Schreiber, Y. Pang, M. B. Brodsky, and H. Sowers, Phys. Rev. Lett. **57**, 2442 (1986).
[4] S. S. P. Parkin, N. More, and K. P. Roche, Phys. Rev. Lett. **64**, 2304 (1990).
[5] J. Unguris, R. J. Celotta, and D. T. Pierce, Phys. Rev. Lett. **67**, 140 (1991).
[6] D. T. Piere, J. A. Stroscio, J. Unguris, and R. J. Celotta, Phys. Rev. B **49**, 14564 (1994).
[7] C. M. Schmidt, D. E. Bürgler, D. M. Schaller, F. Meisinger, and H.-J. Güntherodt, Phys. Rev. B **60**, 4158 (1999).
[8] J. C. Slonczewski, Phys. Rev. Lett. **67**, 3172 (1991).
[9] S. S. P. Parkin, Phys. Rev. Lett. **71**, 1641 (1993).
[10] The pictograph included in the figure indicates the level of sample preparation at which the displayed measurement is performed. Each Fe (Cr) layer is symbolized by a dark gray (light gray) colored rectangle.
[11] A. Schreyer, J. F. Ankner, Th. Zeidler, H. Zabel, M. Schäfer, J. A. Wolf, P. Grünberg, and C. F. Majkrzak, Phys. Rev. B **52**, 16066 (1995).
[12] A. Davies, J. A. Stroscio, D. T. Pierce, and R. J. Celotta, Phys. Rev. Lett. **76**, 4175 (1996).
[13] B. Heinrich, J. F. Cochran, D. Venus, K. Totland, D. Atlan, S. Govorkov, and K. Myrtle, J. Appl. Phys. **79**, 4518 (1996).
[14] R. Schad, P. Beliën, G. Verbanck, V. V. Moshchalkov, Y. Bruynseraede, H. E. Fischer, S. Lefebvre, and M. Bessiere, Phys. Rev. B **59**, 1242 (1999).
[15] D. Olligs, Ph.D. thesis, Universität zu Köln, 1999.
[16] D. E. Bürgler, C. M. Schmidt, J. A. Wolf, T. M. Schaub, and H.-J. Güntherodt, Surf. Sci. **366**, 295 (1996).
[17] D. E. Bürgler and F. Meisinger (unpublished).
[18] D. E. Bürgler, C. M. Schmidt, D. M. Schaller, F. Meisinger, R. Hofer, and H.-J. Güntherodt, Phys. Rev. B **56**, 4149 (1997).
[19] E. E. Fullerton, I. K. Schuller, H. Vanderstraeten, and Y. Bruynseraede, Phys. Rev. B **45**, 9292 (1992).
[20] I.e., the thickness as measured by the quartz microbalance during growth.
[21] K. Temst, M. J. Van Bael, B. Wuyts, C. Van Haesendonck, Y. Bruynseraede, D. G. de Groot, N. Koeman, and R. Griessen, Appl. Phys. Lett. **67**, 3429 (1995).
[22] I. Heyvaert, K. Temst, C. Van Haesendonck, and Y. Bruynseraede, J. Vac. Sci. Technol. B **14**, 1121 (1996).

Downloaded 02 Oct 2001 to 148.6.178.100. Redistribution subject to AIP license or copyright, see http://ojps.aip.org/japo/japcr.jsp